Communications in Physics, Vol. 34, No. 3 (2024), pp. 267-274
DOI: https://doi.org/10.15625/0868-3166/20767

Analysis of ionic defect distribution on perovskite photodetector by temperature-dependent deep level transient spectroscopy

Thi Kim Oanh Vu[1,2,†], **Nguyen Thi Thanh Bao**[1], **Bui Thi Thu Phuong**[1], **Nguyen Ngoc Anh**[1] **and Eun Kyu Kim**[3]

[1]*Institute of Physics, Vietnam Academy of Science and Technology, 10 Dao Tan, Ba Dinh, Hanoi, Vietnam*

[2]*Graduate University of Science and Technology, Vietnam Academy of Science and Technology, 18 Hoang Quoc Viet, Cau Giay, Hanoi, Vietnam*

[3]*Department of Physics and Research Institute for Convergence of Basic Science, Hanyang University, Republic of Korea*

E-mail: [†]vuthikimoanh92@gmail.com

Received 12 May 2024
Accepted for publication 31 July 2024
Published 30 August 2024

Abstract. *In this work we used temperature-dependent deep-level transient spectroscopy for the analysis of the role of additives in high-efficiency organohalide perovskite solar cells prepared by solution-based method. The ionic defect parameters like activation energy, trap density and diffusion constants for each observed ionic species were compared in different solid-state organic–inorganic metal halide perovskites. The obtained results showed that both the Carbonyldiphthalic anhydride and Hexafluoroisopropylidene diphthalic anhydride additives have significantly passivated deep level trap density, consequently enhance perovskite solar cell performance.*

Keywords: perovskite photodetectors;defect passivation;trap density; temperature-dependent deep level transient spectroscopy.

Classification numbers: 68.35.-p; 77.84.-s; 78.60.Fi; 72.80.Jc; 73.61.Ph..

1. Introduction

In 2012, solid-state organic–inorganic metal halide perovskites (PSCs) were reported with a general chemical formula of ABX_3, where A = (methylammonium (MA), $CH_3NH_3^+$; formamidinium (FA), $CH(NH_2)^+$; Cs^+; Rb^+), B = (Pb^{2+}; Sn^{2+}), and halide anion motif X_3 = (I^-; Br^-; Cl^-), and power conversion efficiency (PCE) of 9.7% [1]. Since then, several researchers have attempted to understand and improve their excellent photophysical properties. These include a high optical absorption coefficient, tunable direct bandgap, and fast response speed [2–4]. One of the key breakthroughs in reaching this impressive result is the engineering of the FA^+ based A-site cations with various organic or inorganic elements, such as MA^+ and Cs^+. Besides, the use of Lewis-based precursors such as 4,4′-(Hexafluoroisopropylidene) diphthalic anhydride (6FDA) and 4,4′-Carbonyldiphthalic anhydride (CDA) is also the potential direction to enhance the efficiency of perovskite-based device. A Lewis base is a molecule or ion that can donate a pair of electrons to form a covalent bond with a Lewis acid. 6FDA and CDA can be used as a hole transport material in perovskite photodector, helping to facilitate the movement of positive charges within the devices. It has been shown to enhance the charge transport properties and suppress hysteresis effects [5]. Despite such outstanding performance, the pathway of carriers and defects in perovskite photodetector has not been systematically analyzed. One of the critical challenges for the future development of highly efficient and stable metal-halide perovskite is related to the defects. It has been investigated by several techniques, such as Space- Charge-Limited-Current technology (SCLC) [6], and deep level transient spectroscopy (DLTS). SCLC could be applied to calculate tape density and charge-carrier mobility, but its validity is subject to many assumptions (e.g., no scattering, only one type of charge carrier present). Electrochemical Impedance Spectroscopy (EIS) is a simple but inexact strategy to study the carrier recombination and interfacial resistance. In order to gain an insight into the trapped defects in, and between, each layer and interface, we chose the temperature-dependent deep level transient spectroscopy (T-DLTS) technique, which was successfully used to study defects in PSCs. Functional diphthalic anhydride (4,4′-6FDA and 4,4′-CDA) were used to dope in perovskite solar cell original solution.

In this work, we examine defects in perovskite photodetector prepared via doping techniques. A comparison with different trap densities in control and doped devices was studied. Moreover, the observed ionic defect distributions can explain the large deviations in photovoltaic performance. Alternatively, it also shows the potential to develop tailored passivation strategies to cure certain types of defects.

2. Methodology

Perovskite samples were received from the Department of Energy Science, Sungkyunwan University (SKKU). Firstly 40 nm TiO_2 was grown on FTO, followed by 650 nm perovskite and 130 nm Spiro. 50 nm Au contact was deposited in the Spiro layer by the thermal evaporator. Figure 1 shows a schema of the perovskite solar cells: FTO-coated glass substrate/TiO_2 compact layer/ perovskite/ spiro-OMeTAD/ gold electrode. The bare perovskite layer, the perovskites doped with 0.1% 6FDA and 0.1% CDA were labeled as samples A, B, and C, respectively. The corresponding thickness of each layer is also depicted in Fig. 1. For the Deep Level Transient Spectroscopy measurement, the internal mode of the HP 4280A capacitance meter was used to measure the capacitance-voltage and the time-dependent capacitance transient. The capacitance transients by

the HP 4280A C-meter has measured at 64 points with a sampling time of 50 ms. Measurement temperature was varied in the ranges from 200 K to 375 K continuously by using a closed-cycle refrigerator.

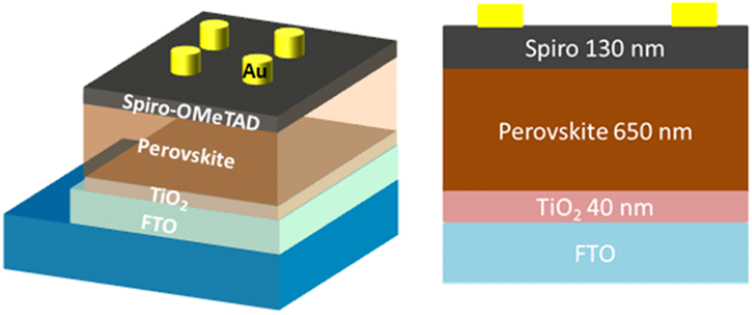

Fig. 1. Schema of the perovskite photodetector structure.

3. Results and Discussions

We have successfully demonstrated the effect of Lewis base additive 6FDA and CDA into perovskite (PS) films on the suppression of defect density by DLTS. For DLTS measurements, the reverse voltages were applied to the Au electrode while capacitance was measured for both samples. Insets of Fig. 2 show the capacitance-voltage (C-V) curves conducted at the 1-MHz frequency with voltage sweeping from 0 to -3 V. These C-V data are widely used to evaluate an arbitrary impurity distribution. The carrier concentration at the edge of the depletion region is expressed from C-V curves by the following equation:

$$N(W) = \frac{2}{q\varepsilon_s}\left[\frac{1}{d(\frac{1}{C^2})/dV}\right] \tag{1}$$

where $N(W)$ is carrier concentration as a function of the depletion width and ε_s is the dielectric constant of semiconductor. The carrier profiles extracted from C-V measurements for samples A, B, and C are illustrated in outer Fig. 2 (a), (b), and (c), respectively. Carriers in samples A and B are rather uniformly distributed in the perovskite layer (density of about 1.9×10^{17} cm^{-3} and 1.4×10^{16} cm^{-3} for samples A and B, respectively), while most of the carriers are distributed in the interface of the spiro-OMeTAD layer and perovskite layer. Sample A has about 10 times higher density than sample B. In sample C, the carriers with an average density of about 3.4×10^{16} cm^{-3} are decreased from about 2×10^{17} cm^{-3} at the surface region to 2×10^{16} cm^{-3} in the depth of the perovskite layer (Fig. 2(c)). From these extracted carrier concentrations, the defect density in the devices could be calculated according to the DLTS results.

To investigate the location and origin of defects in the devices, we conducted DLTS measurements using different measurement voltages. Figure 3 shows the typical DLTS results for sample A, sample B and sample C, respectively, with measurement bias from -1 to -3 V. As clearly shown in Fig. 3(a), under measurement bias of - 1 V, DLTS exhibited two electron traps E2, E3, and a hole trap H1 at about 374 K. When we lowered the bias to – 3 V, hole trap H1 disappeared

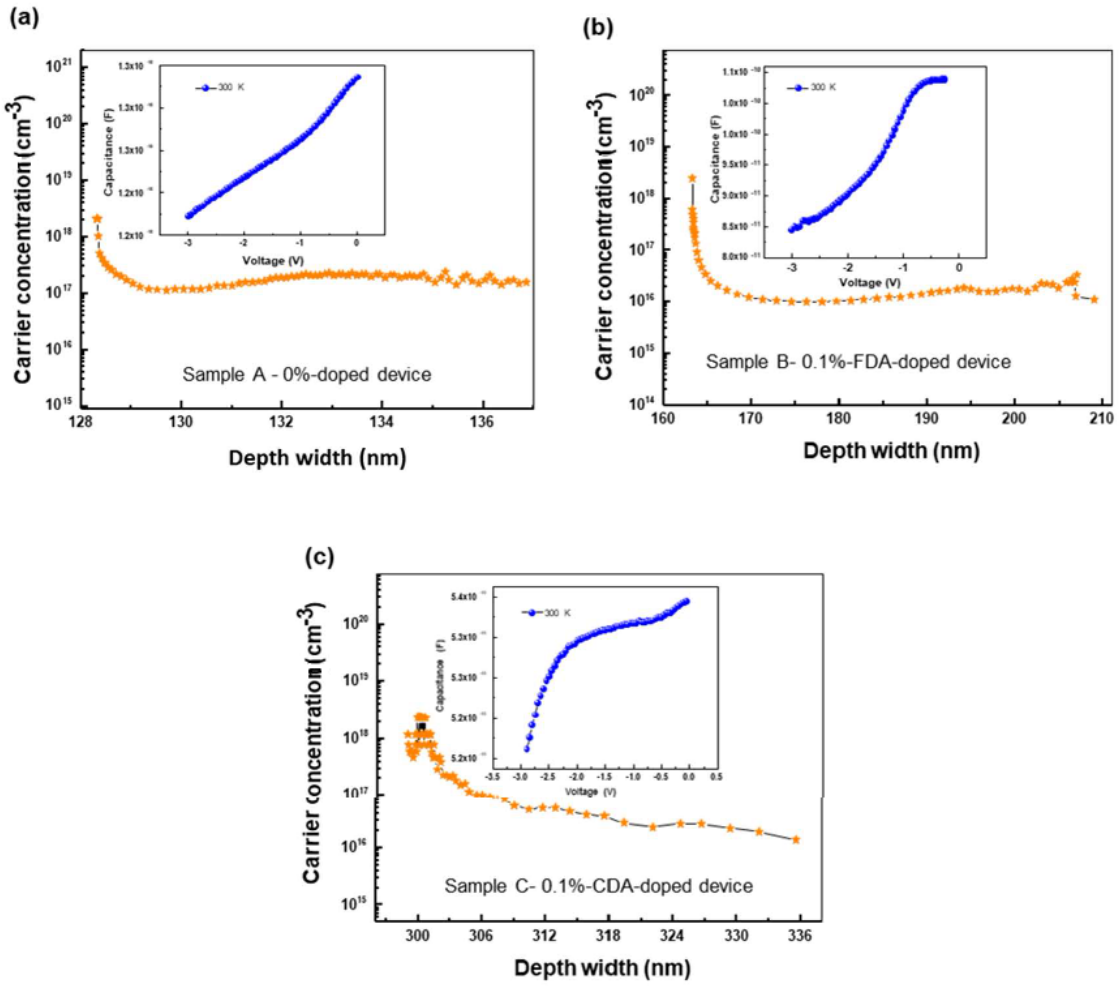

Fig. 2. Carrier concentration as a function of depth determined by capacitance-voltage measurements at 300 K for (a) sample A: non-doped-device, (b) sample B: 0.1%-6FDA-doped-device, and (c) sample C: 0.1%-CDA-doped-device.

while the intensity of two-electron traps increases significantly. This may be because E2 and E3 originate from the PS layer with depletion width at about 136 nm, while H1 may not originate from PS, but it relates to interface states between the PS and spiro-OMeTAD layer. When 6FDA was doped into PS, there was no electron trap was observed (Fig. 3(b)). When the reverse voltage was lowered from – 1 V to – 3 V, the DLTS peak intensity decreased sharply, it indicated that this DLTS peak H1 was rather in the interface between the PS and spiro-OMeTAD layer than in the PS film. The absence of defects in PS films of the 6FDA-doped-device could be attributed to the passivation effect created by forming interactions between uncoordinated lead and Lewis base in the PS. Fig. 3(c) presents the DLTS spectra for the device with doping CDA into PS under measurement voltage of – 1 V and – 3 V. There was no defect observed at the bias of – 1 V, while at the

bias of – 3 V, we could detect two electron traps E1 and E4 which are different with two-electron traps detected in the device without doping. It indicated that these two defects may be formed by interactions between CDA and PS.

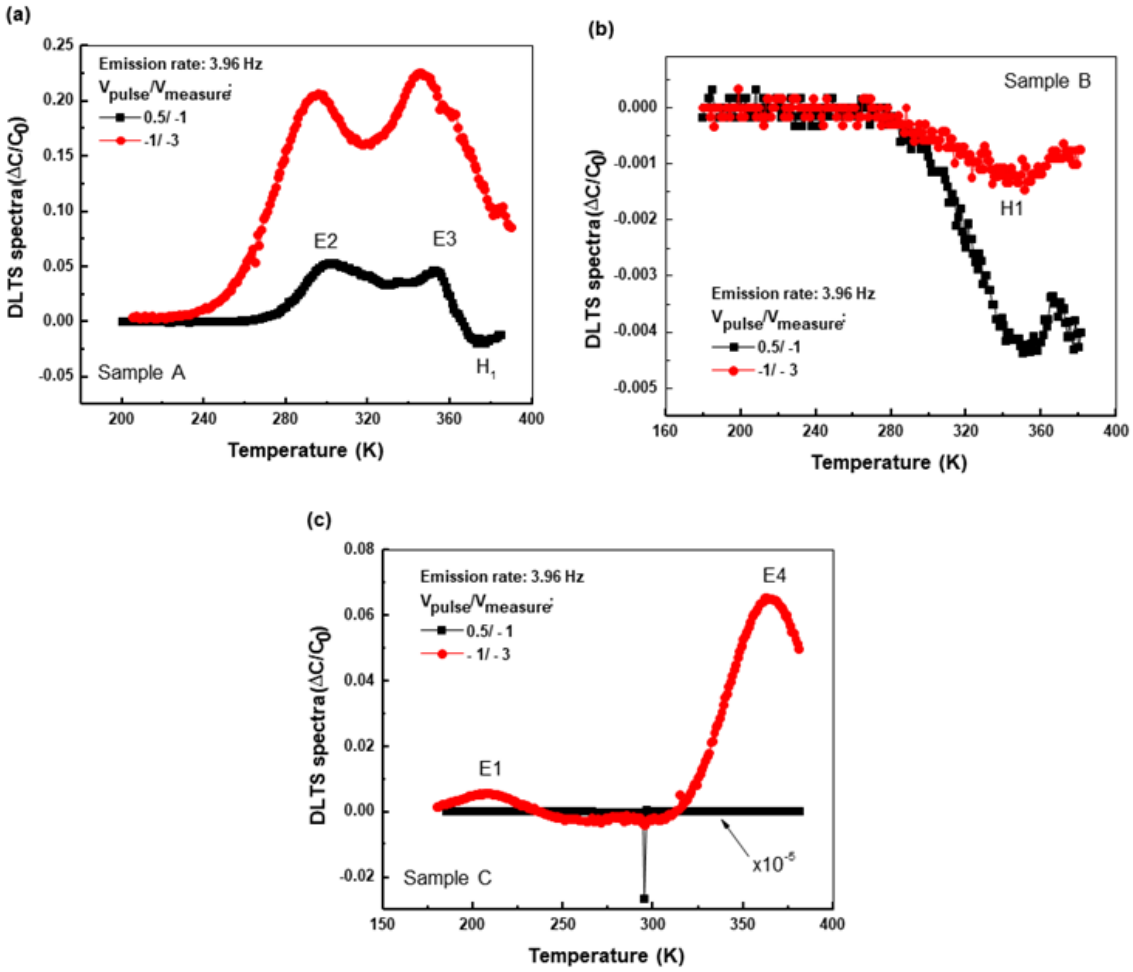

Fig. 3. DLTS spectra with a pulse voltage varied from 0.5 to -1 V and a measurement voltage varied from -1 to -3 V, respectively, for (a) sample A: non-doped-device, (b) sample B: 0.1%-6FDA-doped-device, and (c) sample C: 0.1%-CDA-doped-device. Here, DLTS spectra were obtained under rate window of 3.96 s^{-1} using pulse width of 20 ms with different pulse voltage and measurement voltage, which correspond different depth from the surface.

For rigorous analysis, thermal activation energy and capture cross-section of deep-level traps were obtained by the Arrhenius plot. Using the movement and Arrhenius plot $ln(e_p/T^2)$ versus $1000/T$ as presented in Fig. 4(a) - (c). Sample A (a non-doped device) has three defects E2, E3, and H1 which are located at E_c –0.75 eV, E_c –0.81 eV, and E_v +1.38 eV, respectively. The corresponding capture cross-sections were estimated to be 8.74 x 10^{-15} cm^2, 2.69 x 10^{-14}

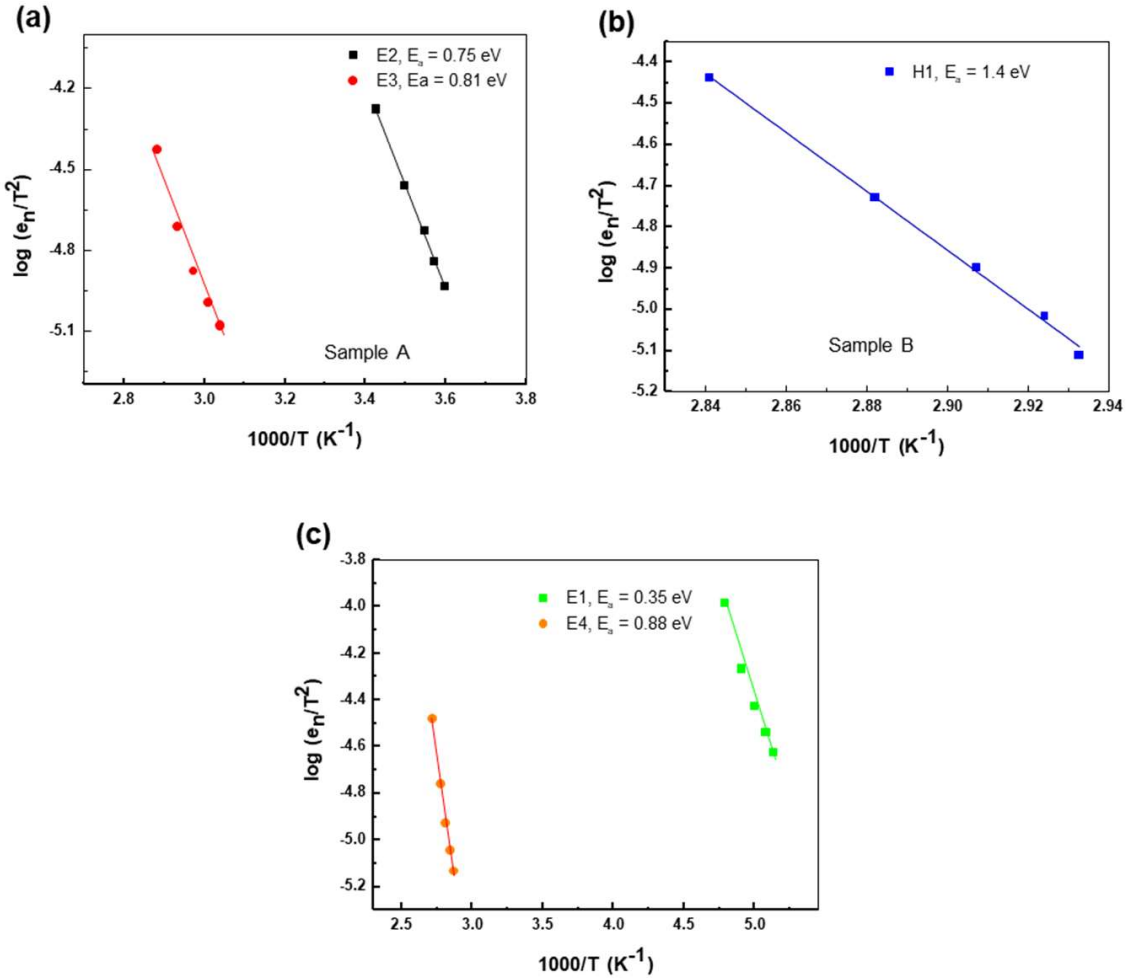

Fig. 4. (a), (b) and (c) show Arrhenius plots for the DLTS signals of Figure 3 (a), (b) and (c), respectively.

cm^2, and 1.03 x 10^{-8} cm^2, respectively. In the preparation of the control-perovskite photodetector, The $(FAPbI_3)_{0.95}(MAPbBr_3)_{0.05}$ perovskite precursor solutions were prepared by dissolving FAI, MABr, PbI_2, and $PbBr_2$ in DMSO/DMF with molar ratio PbI_2 excess. Therefore, the origin of defects in this control-sample could be deep defects in both $MAPbBr_3$ and $FAPbI_3$. First principles calculation was used to investigate the intrinsic defects in $FAPbI_3$ [1]. All possible point defects include vacancies (V_{FA}, V_{Pb}, V_I), interstitials (FA_i, Pb_i, I_i), and antisites (FA_{Pb}, FA_I, Pb_{FA}, Pb_I, I_{FA}, I_{Pb}). Among them, the point defects of iodine such as FA_I, I_{FA}, I_{Pb}, Pb_I which have relatively high formation energy create deep levels in the band gap of $FAPbI_3$. According to Yin *et al.*, [7] the intrinsic point defect of iodine has high formation energy, and the defect trend in $CH_3NH_3PbBr_3$ is like that of intrinsic defects observed in $CH_3NH_3PbI_3$. Therefore, MA_{Br}, Br_{MA}, and Br_{Pb} could create deep states in the band gap of $MAPbBr_3$. Among the above deep defects of $MAPbBr_3$ and

$FAPbI_3$, the energy state of I_{FA} is located about –0.73 eV below the conduction band, and the defect E2 at E_c –0.75 eV observed in the non-doped sample can be correlated with this antisite defect I_{FA}. While defect E3 cannot belong to $MAPbBr_3$ because the DLTS peak's intensity is high but the ratio of $MAPbBr_3$ in solution is small (5%). Though as a transition energy model of $FAPbI_3$ [1], there is no defect with activation energy about E_c-0.81 eV, I_{Pb} exhibits charge transition within the band gap. Especially, I_{Pb} can transit to E_c –0.60 eV and E_c –0.90 eV. Therefore, E2 could be originated from $I_{Pb.}$ E2 is formed by I atoms at the FA sites, while E3 is formed by I atoms at the Pb sites.

Two antisite defects with deep transition levels were formed under Pb-rich conditions. These deep defects could act as recombination centers that trap carriers and shorten the carrier lifetime. The hole trap H1 detected at low depletion width (measure bias of – 1 V) can be formed in the interface between spiro-OMeTAD and PS. Sample B (PS with additive 6FDA) exhibited one hole trap H1 was located at E_v +1.4 eV with a capture cross-section of 8.94×10^{-9} cm^{-3} could have the same origin as H1 in sample A. Sample C (PS with additive CDA) has two electron defects E1 and E4 which are posited at E_c –0.35 eV and E_c –0.88 eV, respectively. The capture cross-section of two of these defects is 6.53×10^{-17} cm^2 and 5.82×10^{-14} cm^2, respectively. According to the charge transition energy level of defects in $FAPbI_3$ cite1 and $MAPbI_3$ [8], the energy state of Pb_I lies at about E_c –0.36 eV, while I_{Pb} can transit to E_c –0.90 eV. Thus E1 and E4 can be related to point defects Pb_I and $I_{Pb.}$ Trap density of each sample was estimated by using DLTS signal intensities and extracted carrier concentration. The trap density in sample A was calculated at 1.03×10^{17} cm^{-3}, which is about 24 times higher than that in sample B ($\sim$4.3 x 10^{15} cm^{-3}), and about 6.4 times higher than that in sample C ($\sim 1.4 \times 10^{16}$ cm^{-3}). This demonstrates successfully that charge traps in perovskite can be suppressed due to Lewis base passivation. The Pb (II) halides (PbX_2) are well-known to be Lewis acids because of the acceptance of iodide anion to form iodoplumbate anions [9,10]. These lead halides can form an adduct with monodentate and bidentate with O-donor, S-donor, and N-donor [11]. The reaction of a Lewis acid (lead halides) with a Lewis base leads to adduct formation where the adduct is linked by sharing electrons originating from the Lewis base to form a coordination compound and passivate the defects [12]. By using the DLTS method, we observed two defects in non-doped-device which originated from I_{FA} and I_{Pb} and were formed under Pb-rich conditions. By adding 0.1%-CDA-Lewis base to perovskite (sample C), CDA reacts with uncoordinated lead and reduces the trap density more than 6 times. Especially, when adding 0.1%-6FDA-Lewis base additive (sample B), almost deep defects in perovskite were passivated. This interaction leads to the formation of a new Lewis acid-base adduct ($C{=}O{-}PbI_2$). For 6FDA-doped perovskite film, not only oxygen but also fluorine can bind to uncoordinated Pb^+ ions which enhance the formation of a Lewis adduct and improve defect passivation functions. These results demonstrate that the doped Lewis base-complexes show an efficient defect passivation effect.

4. Conclusion

In summary, we have successfully demonstrated the effect of Lewis base additive 6FDA and CDA into PS films on suppression of defect density by DLTS. The defect states and densities of perovskite solar cells were investigated by deep level transient spectroscopy. With CDA or 6FDA doping could significantly passivate deep level trap density and enhance perovskite solar cell performance. The obtained results showed that CDA reacts with uncoordinated lead and

reduces the trap density more than 6 times, whereas with 0.1%-6FDA-Lewis base additive, almost deep defects in perovskite were passivated.

Acknowledgement

This research was supported by the Physics development program grant funded by Vietnam Academy of Science and Technology (KHCBVL.06/24-25). EKK acknowledges the financial support by the Korea Evaluation Institute of Industrial Technology (KEIT) grant funded by the Korean goverment (MOTIE) (No.RS-2022-00143570).

Declarations of Interest

The authors declare that they have no known competing financial interests or personal relationships that could have appeared to influence the work reported in this paper.

References

[1] N. Liu and C. Y. Yam, *First-principles study of intrinsic defects in formamidinium lead triiodide perovskite solar cell absorbers*, Phys. Chem. Chem. Phys. **20** (2018) 6800.

[2] N. –G. Park, *Perovskite solar cells: an emerging photovoltaic technology*, Materialstoday **18** (2015) 65.

[3] Y. Liu, L. Zhang, M. Wang, Y. Zhong, M. Huang, Y. Long and H. Zhu, *Bandgap-tunable double-perovskite thin films by solution processing*, Mater. Today **28** (2019) 25.

[4] J. Lim, K. –C. Manuel, Y. –H. Lin, J. M. Ball, N. Sakai, E. A. Duijnstee *et al.*, *Long-range charge carier mobility in metal halide perovskite thin-films and single crystals via transient photo-conductivity*, Nat. Commun. **13** (2022) 4201.

[5] J. Zhu, D. H. Kim, K. D. Kim, D. G. Lee, W. B. Kim, S. W. Chen *et al.*, *All-in-one Lewis base for enhanced precursor and device stability in highly efficient perovskite solar cells*, ACS Energy Lett. **6** (2021) 3425.

[6] V. M. L. Corre, E. A. Duijnstee, O. E. Tambouli, J. M. Ball, H. J. Snaith, J. Lim, L. A. Koster, *Revealing charge carier mobility and defect densities in metal halide perovskites via space-charge-limited current measurements*, ACS Energy Lett. **6** (2021) 1087.

[7] W. J. Yin, T. Shi and Y. Yan, *Unique properties of halide perovskites as possible origins of the superior solar cell performance*, Adv. Mater. **26** (2014) 4653.

[8] Q. Chen, N. D. Marco, Y. Yang, T.-B. Song, C.-C. Chen, H. Zhao *et al.*, *Under the spotlight: The organic–inorganic hybrid halide perovskite for optoelectronic applications*, Nano Today **10** (2015) 355.

[9] H. Krautscheid and F. Vielsack, *$[BuN(CH_2CH_2)_3NBu]_3[Pb_5I_{16}] \cdot 4DMF$ – an iodoplumbate anion with approximately D5h-symmetry*, Z. Anorg. Allg. Chem. **626** (2000) 3.

[10] H. Krautscheid and F. Vielsack, *Discrete and polymeric iodoplumbates with Pb_3I_{10} building blocks: $[Pb_3I_{10}]^{4-}$, $[Pb_7I_{22}]^{8-}$, $[Pb_{10}I_{28}]^{8-}$, $1_\infty[Pb_3I_{10}]^{4-}$ and $2_\infty[Pb_7I_{18}]^{4-}$*, J. Chem. Soc., Dalton Trans. (1999) 2731.

[11] I. Wharf, T. Gramstad, R. Makhija and M. Onyszchuk*, Synthesis and vibrational spectra of some lead(I1) halide adducts with 0-, S-, and N-donor atom ligands*, Can. J. Chem. **54** (1976) 3430.

[12] G. Yang, P. Qin, G. Fang and G. Li, *A lewis base-assisted passivation strategy towards highly efficient and stable perovskite solar cells*, Sol. RRL, **2** (2018) 1800055.